Transition rates of high-spin states in ^{56}Co and ^{56}Fe: Possible coexistence of prolate- and oblate-like configurations in ^{56}Fe†

D. G. Sarantites, J. Urbon, and L. L. Rutledge, Jr.
Department of Chemistry, Washington University, St. Louis, Missouri 63130
(Received 4 March 1976)

The decay properties of the high-spin states in ^{56}Co and ^{56}Fe have been investigated via the ^{54}Fe$(\alpha,pn)^{56}$Co*(γ) and ^{54}Fe$(\alpha,2p)^{56}$Fe*(γ) reactions in the energy range 20.4–29.5 MeV. From measurements of excitation functions and angular distributions of individual γ rays with a Ge(Li)-NaI(Tl) anti-Compton spectrometer, and from $\gamma\gamma$-coincidence experiments new levels in ^{56}Co have been identified at 2282.6 (7_1^+), 2371.9 (6_1^+), 3638.0 (8_1^+), 4180.2 (9_1^+), and 5274.6 (10_1^+) keV with the deduced J^π values in parentheses. Similarly levels in ^{56}Fe have been confirmed at 3388.4 (6_1^+), 3755.8 (6_2^+), 4700.6 (7_1^+), 5255.3 (8_1^+), and 5626.8 (8_2^+) keV and the J^π values in parentheses have been deduced. The angular distributions in conjunction with the associated attenuation factors were analyzed to yield multipole mixing ratios $\delta(E2/M1)$. The mean lifetimes τ of these states were also carefully measured by extrapolation to the detection threshold of the effective mean lifetimes extracted from Doppler-broadened line shapes obtained at four bombardment energies between 20.4 and 29.5 MeV. The values obtained in ^{56}Co are 2282.6 keV (>2000 fs), 2371.9 keV (60 ± 30 fs), 3638.0 keV (80^{+40}_{-30} fs), 4180.2 keV (590 ± 60 fs), and 5274.6 keV (60^{+40}_{-20} fs); and those in ^{56}Fe are 3388.4 keV (>2000 fs), 3755.8 keV (180^{+40}_{-30} fs), 4700.6 keV (120 ± 40 fs), 5255.3 keV (500 ± 50 fs), and 5626.8 keV (100^{+40}_{-20} fs). For most of the transitions from the high-spin states in ^{56}Co and ^{56}Fe $B(\Lambda)$ values were obtained. The results for ^{56}Fe are compared with recent calculations based on the aligned coupling scheme indicating possible coexistence of quasiband structures with prolate- and oblate-like configurations. The results for ^{56}Co are compared with other recent shell-model calculations and good agreement is observed.

[NUCLEAR REACTIONS ^{54}Fe$(\alpha,pn)^{56}$Co*(γ) and ^{54}Fe$(\alpha,2p)^{56}$Fe*(γ), E = 21–30 MeV, enriched targets. Measured, E_γ, I_γ, $I_\gamma(\theta)$, $\sigma(E)$, $\Delta\overline{E}_\gamma(E,\tau)$, $\gamma\gamma$ coin., deduced levels in ^{56}Co and ^{56}Fe, J, π, branching ratios, τ_{level}, $\delta(E2/M1)$, $B(E2)$ and $B(M1)$ values; Ge(Li) detectors, Ge(Li)-NaI(Tl) anti-Compton spectrometer, 2.2. keV at 1332.5 keV.]

I. INTRODUCTION

In the past several years considerable effort has been devoted to the experimental and theoretical study of the decay properties of the low-lying levels in $^{56}_{26}Fe_{30}$ and $^{56}_{27}Co_{29}$ because of their proximity to the doubly closed shell that occurs in $^{56}_{28}Ni_{28}$. Such nuclei near closed shells can be described in terms of a few valence particles with rather pure shell model configurations. This is particularly true for the high-spin states. Furthermore, transition rates from such high-spin states give information about the effective charges of the multipole operators. Recent calculations by Horie and Ogawa[1] in the $N=29$ nuclei have provided the effective proton-neutron matrix elements and predictions of the properties of the high-spin states in ^{56}Fe based on these calculations have been reported by Poletti *et al.*[2]

More recently, shell-model calculations for energies and $B(\Lambda)$ values for the low-spin states in ^{56}Co have been done by McGrory.[3] The level energies from these calculations have been compared with experiment by Samuelson *et al.*[4] and by Schneider and Daehnick.[5] The calculated[3] $B(\Lambda)$ values have been compared with experiment very recently by Barker and Sarantites[6] and by Moazed *et al.*[7]

During the preparation of this manuscript Tanaka and Sheline[8] reported results of some calculations indicating that quasiband structures in nuclei near doubly closed shells can be described by the aligned coupling scheme (ACS) wave functions. In particular they reported calculated spectra and transition rates for ^{56}Fe corresponding to configurations with prolate and oblate shapes. It will be shown that the predicted spectra reproduce the position of the high-spin states in ^{56}Fe and indicate the possible coexistence of oblate- and prolate-like configurations.

The earlier experimental studies of the properties of the states in ^{56}Co have been summarized in the extensive ^{56}Fe$(p,n)^{56}$Co study of Samuelson *et al.*[4] Lifetime measurements for the lower-spin states in ^{56}Co obtained by the Doppler-shift attenuation technique have been reported by Barker

and Sarantites[6] using the ^{56}Fe$(p,n\gamma)$ reaction and by Moazed *et al.*[7] using the ^{54}Fe$(^3$He$,p\gamma)$ reaction.

The properties of the low-spin states in ^{56}Fe investigated in a wide variety of reactions have been summarized by Rao.[9] Levels up to 6_1^+ in ^{56}Fe have been recently reported by Poletti *et al.*[2] from a ^{51}V$(^7$Li$,2n)^{56}$Fe study at 25 MeV.

In this work the ^{54}Fe$(\alpha,pn)^{56}$Co and ^{54}Fe$(\alpha,2p)$-^{56}Fe reactions have been employed in the energy range 20.4–29.5 MeV in order to study the high-spin states in the ^{56}Co and ^{56}Fe product nuclei. From this work levels at 2282.6 (7_1^+), 2371.9 (6_1^+), 3638.0 (8_1^+), 4180.2 (9_1^+), and 5274.6 (10_1^+) keV have been identified in ^{56}Co and were assigned the J^π values given in parentheses. The previously reported[2] levels at 3388.4 (6_1^+), 3755.8 (6_2^+), 4700.6 (7_1^+), 5255.3 (8_1^+), and 5626.8 (8_2^+) in ^{56}Fe have been confirmed and definite assignments of the J^π values given in parentheses were made. A careful analysis of the observed angular distributions has yielded definite spin assignments for all levels and provided multipole mixing ratios for most of the transitions involved in the decay of the high-spin states in ^{56}Co and ^{56}Fe. A systematic study of the Doppler-shift attenuation with bombardment energy has permitted the measurement of many subpicosecond lifetimes for the decay of these high-spin states. From these results the $B(\Lambda)$ values for most of the transitions were obtained and were compared with recent shell-model calculations.

II. EXPERIMENTS AND RESULTS

In this work the external beam facility[10] of the Washington University cyclotron provided the 21.0–30.0-MeV ^{4}He^{++} beams required. For singles γ-ray measurements under Compton suppression a small cylindrical scattering chamber was employed. A surface barrier Si diode was positioned at 90° to the beam to monitor the scattered charged particles. With the exception of the γ-ray measurements at 90°, the beam after passing through the target was stopped in a narrow lead strip at the back of the scattering chamber. The good collimation of the anti-Compton spectrometer permitted spectra to be taken down to 20° to the beam without interference from γ rays produced in the lead beam stop.

For $\gamma\gamma$-coincidence experiments a different small scattering chamber was used that permitted two Ge(Li) detectors to be placed at 55° to the beam on either side at a distance of ~4 cm from the target. In this arrangement the beam was stopped in a lead plate at the end of a 5 m long Faraday cup to reduce background radiation.

The target employed was a 5.0-mg/cm^2 foil of ^{54}Fe enriched to 96% in mass 56 and it was prepared by rolling of the metal. The target was positioned at 30° or 45° to the beam direction.

A. Detection equipment

In this work two Ge(Li) detectors were employed which had 5.3 and 6.7% efficiency [compared with a 7.6-cm × 7.6-cm NaI(Tl) detector at 25 cm for a 1332-keV γ ray] and 2.6 and 2.2 keV full width at half maximum at 1332 keV, respectively. Both detectors were at different times employed in an anti-Compton arrangement[11] which gave a peak-to-Compton ratio of 100 : 1 for a 1275-keV γ ray. This anti-Compton spectrometer and its shielding was located on an angular correlation table that permitted spectra to be taken between 0°–90° to the beam direction.

B. γ-ray energy measurements

The energies of the γ rays from the $(\alpha,pn\gamma)$ and $(\alpha,2p\gamma)$ reactions on ^{54}Fe were measured from γ-ray spectra recorded at 90° to the beam direction at 30 MeV of α-bombardment energy. These spectra were taken in the presence of standard sources of ^{57}Co, ^{133}Ba, ^{207}Bi, ^{137}Cs, ^{54}Mn, ^{22}Na, ^{60}Co, and ^{56}Co in different combinations. These sources were prepared thin and were mounted in front of the collimator of the anti-Compton spectrometer outside the lead shield. The small nonlinearity of this system was well accounted for by a third order polynomial function of energy vs channel number.

A Compton-suppressed spectrum of the γ rays from a 30-MeV bombardment taken at 90° to the beam direction is shown in Fig. 1. The γ-ray peaks labeled by p, $2p$, pn, $2pn$, α, αn, αp, b, and u are believed to be associated with the (α,p), $(\alpha,2p)$, (α,pn), $(\alpha,2pn)$, (α,α'), $(\alpha,\alpha'n)$, $(\alpha,\alpha'p)$ reactions, background radiations, and unidentified radiations, respectively. The large Doppler broadening for some of the high energy transitions shown is quite apparent from the spectrum of Fig. 1.

The energies of the γ rays assigned in this work to the decay of levels in ^{56}Co and ^{56}Fe are summarized in the fifth column of Table I. The level energies and J^π values assigned in this work are summarized in the second and third column in Table I. In the fourth column each transition is identified for convenience by the level numbers given in the first column of Table I.

C. Relative γ-ray excitation functions

The relative excitation functions of the γ rays from the (α,pn) and $(\alpha,2p)$ reactions on ^{54}Fe have

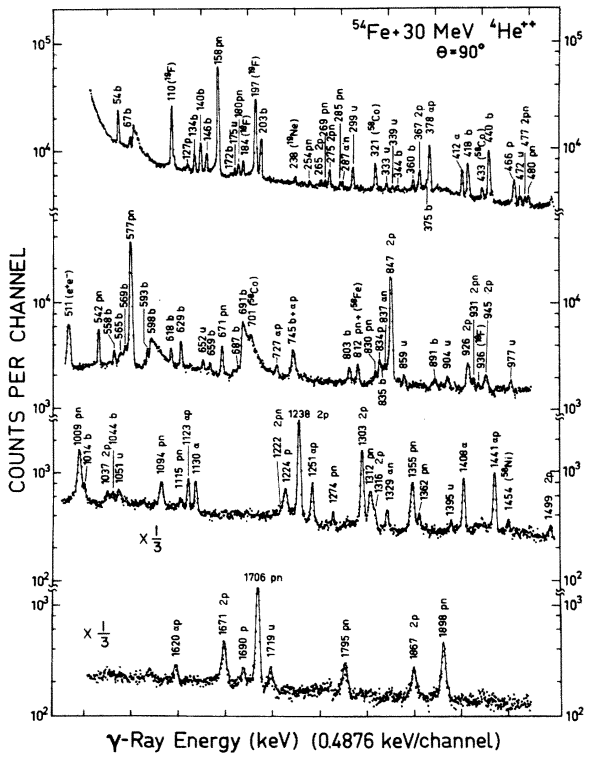

FIG. 1. Compton-suppressed spectrum of the γ rays observed at 90° to the beam in a 29.5-MeV α bombardment of ^{54}Fe. The γ rays are labeled in keV. Peaks labeled by p, $2p$, pn, $2pn$, α, αn, and αp are believed to be associated with the (α,p), $(\alpha,2p)$, (α,pn), $(\alpha,2pn)$, (α,α'), $(\alpha,\alpha'n)$, and $(\alpha,\alpha'p)$ reactions, while those labeled by b and u are background and unidentified radiations, respectively.

been determined for the bombardment energies of 20.4, 23.4, 26.5, and 29.6 MeV. These were measured from Compton-suppressed spectra taken at 55° to the beam direction. The γ-ray intensities thus obtained are summarized in columns 6–9 in Table I and are expressed relative to the 576.64-keV transition in ^{56}Co and the 846.8-keV transition in ^{56}Fe taken as 100 at each bombardment energy. The last column in Table I gives the branching ratios in percent for the transitions from each level, obtained as weighted averages from the results summarized in columns 6 through 9.

The relative excitation functions of the γ rays from levels that were observed to decay by more than one transition have similar shapes within experimental error. In order to depict the characteristic dependence of the excitation function on the angular momentum J^π of each observed level, the relative excitation functions for the cumulative formation of each level are plotted in Fig. 2. The solid curves through the data points have been drawn to guide the eye, but such a dependence of J is predicted by calculations based on the compound-statistical theory for nuclear reactions.[12] The assignment of J^π values are based primarily on results from angular distribution measurements with strong support from the evidence from the excitation functions shown in Fig. 2 as discussed below.

D. $\gamma\gamma$-coincidence experiment

The coincidence relationships of the γ rays observed in the present reactions are essential in establishing the decay schemes of the states in ^{56}Co and ^{56}Fe. The coincidence relationships were established in an experiment at 29.6 MeV. In this experiment fast crossover timing was employed and ≃130-ns resolving time at 1/10 height was obtained. The two Ge(Li) detectors were positioned at 55° on each side of the beam with about 1 cm of Pb absorber between the detectors to reduce the crystal-to-crystal scattering. With a total coincidence rate of ≃350 counts/s and singles rates of ≃4000 and ≃7000 counts/s a total random coincidence rate of 5% was observed. A total number of $\simeq 2.0\times10^7$ coincidence events with 100% coincidence efficiency between 60 and 2000 keV, were recorded and processed.

The data were recorded on magnetic tape in the event by event form in a 4096×4096 channel configuration. The sorting of the data was done with the aid of a program written for an IBM-360 Model 65 computer. Gates were placed on all observed peaks and selected adjacent Compton backgrounds. The Compton background spectra were properly normalized and subtracted from the spectra gating the peaks. The γ rays thus observed in coincidence are summarized in Table II. On the basis of the $\gamma\gamma$-coincidence relationships the decay schemes shown in Figs. 3 and 4 were constructed for the decay of levels in ^{56}Co and ^{56}Fe. All the γ rays listed in Table II have been assigned in ^{56}Co and ^{56}Fe but some of the transitions corresponding to the decay of low-spin states, previously assigned,[4,6] for simplicity are not included in Figs. 3 and 4.

E. γ-ray angular distributions

The angular distributions of all but the few weakest transitions observed in ^{56}Co and ^{56}Fe have been measured at 29.5 MeV of α-bombardment energy. In this experiment Compton-suppressed γ-ray spectra were recorded twice for a short time (~5 min) at each of the angles 90, 75, 70, 60, 55, 45, 30, and 20° to the beam direction. In these measurements the beam was monitored by re-

TABLE I. Summary of level energies, J^{π} values, γ-ray energies, relative γ-ray yields, and branching ratios for transitions in ^{56}Co and ^{56}Fe determined in this work via the ^{54}Fe(α, pn) and ^{54}Fe($\alpha, 2p$) reactions.

Level No.	Level energy (keV)		J^{π}	Transition	γ-ray energy (keV)		Relative γ-ray intensities [a] for E_{α} (MeV) 20.4		23.4		26.5		29.5		Branching (%)	
									^{56}Co							
0	0		4_1^+													
1	158.38	10[b]	3_1^+	1→0	158.38	10	70.6	18	44.2	6	37.0	4	28.0	4	100.0	
2	576.50	7[b]	5_1^+	2→0	576.64	19	100		100		100		100		100.0	
3	829.58	6[b]	4_2^+	3→2	252.9	2	0.24	22	0.21	10	0.13	7	0.18	8	1.6	5
				3→1	671.4	4	17.0	12	9.4	6	7.5	4	6.0	5	82	5
				3→0	830.1	2			1.3	4	1.5	3	1.6	4	16	3
4	970.25	1	2_1^+	4→1	811.8	1	6.8	15	8.9	7	6.3	5	6.1	7	99.7	56[c]
				4→0	970.4	2	<0.9		<0.3		<0.3		<1.0		0.30	5[c]
5	1009.17	6	5_2^+	5→3	179.5	2	1.01	20	0.94	13	0.83	9	0.86	12	2.8	5
				5→2	432.7	2	2.7	6	2.5	3	2.1	2	2.2	3	7.4	6
				5→0	1009.3	2	42	2	30	1	26	1	24	1	89.8	20
6	2282.6	2	7_1^+	6→2	1706.1	1	19	2	60	2	72	2	68	2	100.0	
7	2371.9	2	6_1^+	7→3	1362.0	5	6.2	10	4.2	7	3.3	6	4.4	9	28	3
				7→2	1795.4	2	5.4	18	8.2	12	10.1	10	10.9	15	72	6
8	3638.0	2	8_1^+	8→6	1355.4	1	8.9	20	16	2	27	1	28	2	100.0	
9	4180.2	2	9_1^+	9→8	542.0	1	1.6	4	3.2	5	8.1	5	9.5	6	27	1
				9→6	1898.0	3	6.1	3	11	2	20	1	26	2	73	3
10	5274.6	3	10_1^+	10→9	1094.4	1			1.0	5	6.7	10	12.0	15	100.0	
									^{56}Fe							
0			0^+													
1	846.8	1	2_1^+	1→0	846.8		100		100		100		100		100	
2	2085.1	1	4_1^+	2→1	1238.20	7	74	2	92	2	96	2	93	2	100	
3	3122.9	1	4_2^+	3→2	1037.8	1	0.92	18	1.12	22	1.07	15	1.9	3	99.2	7[d]
				3→1	2276.3	2									0.78	4[d]
4	3388.4	2	6_1^+	4→3	265.5	2					0.36	13	0.86	22	1.3	3
				4→2	1303.4	1	27	1	47	2	51	2	52	2	98.7	40
5	3755.8	3	6_2^+	5→4	367.0	1	6.5	7	6.0	3	5.0	3	4.9	3	18	1
				5→3	1670.8	4	9.5	10	16	1	19	1	21	2	82	3
6	4700.6	3	7_1^+	6→5	944.7	2			1.5	2	3.2	5	4.6	8	16	2
				6→4	1312.2	1	3.9	5	14	1	17	1	22	2	84	4
7	5255.3	3	8_1^+	7→5	1499.3	3			2.5	6	4.9	9	4.7	9	27	3
				7→4	1867.1	2	1.4	6	8.2	9	10	1	13	1	73	4
8	5626.8	3	8_2^+	8→6	926.2	1			2.9	5	6.2	6	10.4	10	91.7	14
				8→4	2238	2							0.9	2	8.3	20

[a] Values deduced from spectra taken at 55°.
[b] Values obtained as weighted average of the level energies from this work and Ref. 6.
[c] Values from Ref. 6.
[d] Values from Ref. 9.

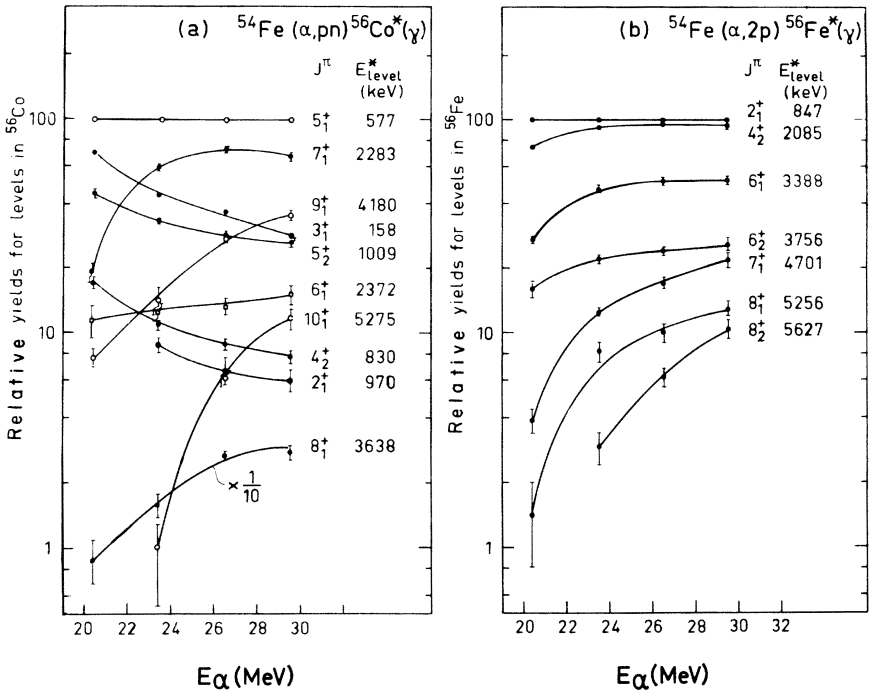

FIG. 2. Excitation functions for the cumulative formation of levels by the ^{54}Fe(α,pn)^{56}Co*(γ) and ^{54}Fe(α,$2p$)^{56}Fe*(γ) reactions plotted relative to the 576.5- and 846.78-keV levels in ^{56}Co and ^{56}Fe taken as 100, respectively. The levels have been labeled by their energies in keV and by their J^π values (see text). The lines through the data have been drawn to guide the eye.

TABLE II. Summary of the observed $\gamma\gamma$ coincidence relationships in the decay of levels in ^{56}Co and ^{56}Fe populated by the (α, pn) and (α, $2p$) reactions on ^{54}Fe at $E_\alpha = 29.5$ MeV.

γ-ray energy in the Ge(Li) gate (keV)	γ-ray energy observed in the Ge(Li) coincidence spectrum (keV)
	^{56}Co
158	285, 480, 671, 812
542	577, 1094, 1355, 1706
577	321, 542, 1094, 1355, 1706, 1795, 1898
1009	1362
1094	542, 577, 1355, 1706, 1898
1355	542, 577, 1094, 1706
1362	1009
1706	542, 577, 1094, 1355, 1898
1795	577
1898	577, 1094, 1706
	^{56}Fe
367	847, 1238, 1303
847	367, 926, 945, 1038, 1238, 1303, 1312, 1499, 1671, 1867
926	847, 945, 1238, 1303, 1312
1238	367, 847, 926, 945, 1038, 1303, 1312, 1499, 1671, 1867
1303	367, 847, 926, 1867
1312	847, 926, 1238, 1303
1671	847, 945, 1238, 1499
1867	847, 1238, 1303

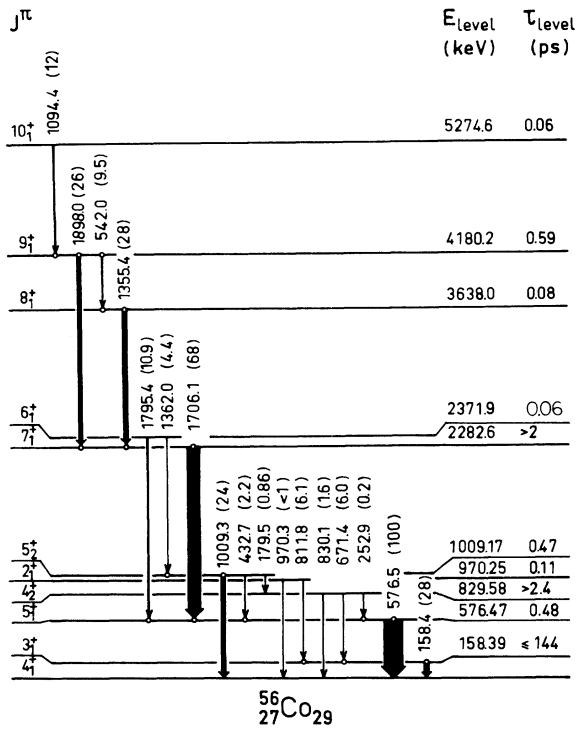

FIG. 3. Proposed scheme for the decay of high-spin levels in ^{56}Co populated in the ^{54}Fe$(\alpha,pn)^{56}$Co*(γ) reaction up to 29.5 MeV. The level and transition energies are given in keV and the relative intensities in parentheses refer to the 29.5 MeV excitation. The mean lifetimes for the decay of these levels are given in ps.

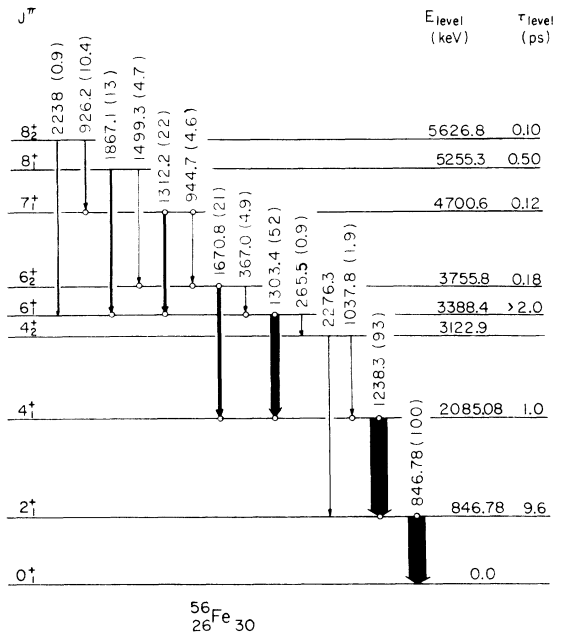

FIG. 4. Proposed scheme for the decay of high-spin levels in ^{56}Fe populated in the ^{54}Fe$(\alpha,2p)^{56}$Fe*(γ) reaction up to 29.5 MeV. The level and transition energies are given in keV and the relative intensities in parentheses refer to the 29.5 MeV excitation. The mean lifetimes for the decay of these levels are given in ps.

cording the charged particles with a surface barrier detector at 90° to the beam. In this way the angular distribution of the 158.38- and 576.5-keV γ rays were first determined and then used as internal monitors for the other distributions from additional spectra recorded with good statistics. The distributions thus obtained are shown in Fig. 5 and are plotted versus $\cos^2\theta_d$.

The angular distributions shown in Fig. 5 were analyzed to give evidence for J^π assignments and to extract multipole mixing ratios $\delta(E2/M1)$. The procedure outlined in detail in Ref. 13 was followed for this purpose. The A_2 and A_4 coefficients from a least-squares fit of the data to the function of Eq. (1) in Ref. 13 are given in columns 3 and 4 of Table III. The analysis of the measured γ-ray distributions in terms of the attenuation coefficients[13] $\alpha_2(J_1)$ is facilitated in this case by the presence of the two well established $E2$ transitions, namely, $2_1^+ \rightarrow 0_1^+$ at 846.78 and $4_1^+ \rightarrow 2_1^+$ at 1238.2 keV in ^{56}Fe. The search for a χ^2 minimum in varying δ and σ, the Gaussian width parameter for the population of the magnetic substates,[13] with the aid of the code SAGA[14] (see also Ref. 13), gave unique minima for these two transitions for essentially vanishing $\delta(M3/E2)$ values. Five additional distributions have A_2 and A_4 values characteristic of stretched E_2 transitions (see Table III). From these distributions and in conjunction with the excitation functions as discussed below definite J^π assignments could be made for all the levels observed. In Fig. 6 the solid circles are the $\alpha_2(J_1)$ attenuation coefficients (Table III) plotted versus J_1 for the stretched transitions. The open circles are the $\alpha_2(J_2)$ values for mixed $M1+E2$ values corresponding to (σ,δ) values in a χ^2 search with SAGA[14] that gave a minimum corresponding to $\alpha_2(J)$ near the empirically drawn line in Fig. 6. The σ and $\delta(L+1/L)$ values obtained in the present analysis are given in columns 6 and 8 of Table III. The last column gives the $\delta(E2/M1)$ values obtained corresponding to the deduced $J_i^\pi \rightarrow J_f^\pi$ sequence given in the fifth column of Table III.

F. Doppler-broadened line shape measurements

The mean lifetimes of all but two of the high-spin states in ^{56}Co and ^{56}Fe observed in this work were measured from a systematic analysis of the Doppler-broadened line shapes (DBLS) of the observed γ rays at four bombardment energies of

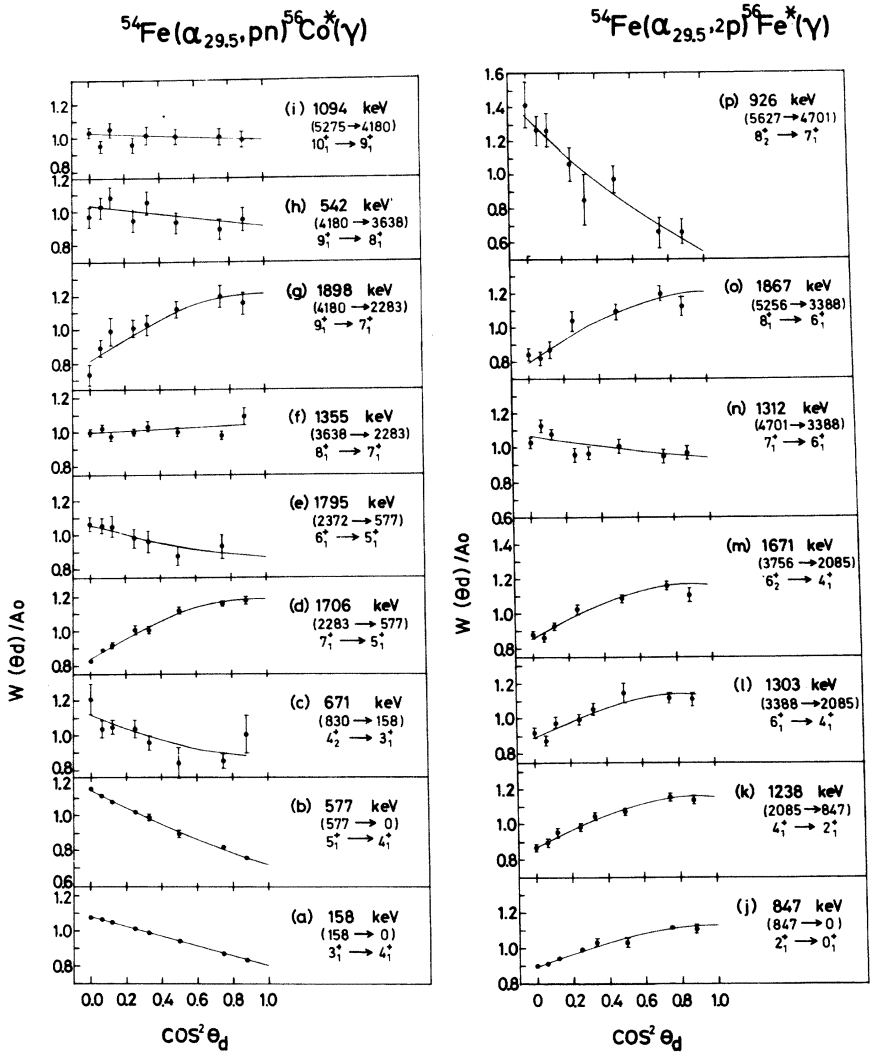

FIG. 5. Singles angular distributions of the γ rays indicated in keV for the transitions identified by the level energies given in parentheses in keV. The solid curves are the theoretical distributions for the σ and δ values (Table III) that gave the minimum χ^2 fit to the data for the most likely spin sequence indicated.

20.4, 23.4, 26.5, and 29.5 MeV. The method of measurement consists of extracting an effective lifetime as a function of bombardment energy and extrapolating to an effective threshold energy at which the γ feeding to the level in question goes to zero. Lifetimes extracted by this technique have been reported earlier by Sarantites *et al.*[13,15] The effective threshold for the population of high-spin states in light nuclei ($A \sim 60$) via (α, pn) and $(\alpha, 2p)$ reactions is reasonably well approximated by the bombardment energy below which the γ rays from feeding transitions to the level in question cannot be detected and is several MeV above the real threshold. For cases where feeding transitions are not observed, a reasonable effective threshold would be the energy below which the γ ray in question cannot be detected. This is demonstrated in Fig. 7 where the fraction of population of four levels in ^{56}Fe and ^{56}Co by observed γ rays from levels above is plotted as a function of bombardment energy. It is seen that these fractions vary with energy in a nearly linear fashion and become zero at the energies indicated by the vertical arrows in Fig. 7. These energies are considerably higher than the true thresholds of the levels in question, but they are located in a region where the level cross sections decrease rapidly with decreasing energy (a factor of ~5 per MeV).

Under the kinematic conditions applicable to this work, for measurements near the threshold of each state, the Doppler shift observed for the very short-lived transitions resulted in complete-

TABLE III. Summary of angular distribution coefficients, angular distribution attenuation coefficients, multipole mixing ratios, and J^π values obtained in this work for high J transitions in ^{56}Co and ^{56}Fe following the ^{54}Fe$(\alpha,pn)^{56}$Co*(γ) and ^{54}Fe$(\alpha,2p)^{56}$Fe*(γ) reactions at 29.5 MeV.

Level energy (keV)	Transition energy (keV)	A_2	A_4	$J_i^\pi \rightarrow J_f^\pi$	σ	α_2	$\delta(L+1/L)$	$\delta(E2/M1)$ or multipolarity
				^{56}Co				
158.38	158.38	−0.184 13	0.020 14	$3_1^+ \rightarrow 4_1^+$	2.00	0.32 ± 0.02	−0.27 ± 0.04	−0.27 ± 0.04
576.50	576.50	−0.280 26	0.040 35	$5_1^+ \rightarrow 4_1^+$	2.68	0.43 ± 0.04	+0.16 ± 0.06	+0.16 ± 0.06
829.58	671.4	−0.184 35	0.104 57	$4_2^+ \rightarrow 3_1^+$	2.40	0.37 ± 0.15	+0.09 ± 0.12	+0.09 ± 0.12
2282.6	1706.1	0.263 34	−0.078 36	$7_1^+ \rightarrow 5_1^+$	2.52	0.67 ± 0.09 [a]	0.035 ± 0.035	$E2$
2371.9	1795.4	−0.100 41	0.113 51	$6_1^+ \rightarrow 5_1^+$	2.59	0.56 ± 0.22	−0.03 ± 0.05 or >29	−0.03 ± 0.05
3638.0	1355.4	−0.010 30	0.005 48	$8_1^+ \rightarrow 7_1^+$	2.40	0.76	−0.15 ± 0.04	−0.15 ± 0.04
4180.2	542.0	−0.068 44	0.004 68	$9_1^+ \rightarrow 8_1^+$	2.12	0.85	−0.05 ± 0.09	−0.05 ± 0.09
	1898.0	0.279 46	−0.167 57	$9_1^+ \rightarrow 7_1^+$	2.12	0.85 ± 0.14 [a]	0.066 ± 0.066	$E2$
5274.6	1094.4	−0.020 30	0.00 4	$10_1^+ \rightarrow 9_1^+$	2.2	0.84 ± 0.12	−0.13 ± 0.05	−0.13 ± 0.05
				^{56}Fe				
846.78	846.78	0.184 20	−0.029 27	$2_1^+ \rightarrow 0_1^+$	1.56	0.26 ± 0.03	$0.0^{+0.2}_{-1.1}$	$E2$
2085.08	1238.20	0.217 14	−0.085 27	$4_1^+ \rightarrow 2_1^+$	2.26	0.43 ± 0.03	0.00 ± 0.09	$E2$
3388.4	1303.4	0.219 30	−0.123 31	$6_1^+ \rightarrow 4_1^+$	2.70	0.53 ± 0.09 [a]	0.09 ± 0.08	$E2$
3755.8	367.0	0.244 40	0.020 45	$6_2^+ \rightarrow 6_1^+$	2.50	0.54 ± 0.09	0.07 ± 0.09	0.07 ± 0.12
	1670.8	0.227 35	−0.090 48	$6_2^+ \rightarrow 4_1^+$	2.42	0.60 ± 0.09 [a]	0.06 ± 0.08	$E2$
4700.6	1312.2	−0.134 37	0.087 45	$7_1^+ \rightarrow 6_1^+$	2.87	0.59 ± 0.10	−0.077 ± 0.08	−0.08 ± 0.08
5255.3	1867.1	0.277 26	−0.119 66	$8_1^+ \rightarrow 6_1^+$	2.42	0.78 ± 0.07 [a]	+0.05 ± 0.07	$E2$
5626.8	926.2	−0.492 58	+0.08 26	$8_2^+ \rightarrow 7_1^+$	2.88	0.66 ± 0.08	0.25 ± 0.10	+0.25 ± 0.10

[a] Values obtained assuming $\delta(M3/E2)=0$.

ly shifted γ peaks. Examples of this are shown in Figs. 8(a), 8(c), 8(e), and 8(g). When the bombardment energy is increased, population via other unknown transitions apparently occurs and this in most cases was observed as a small unshifted peak [Figs. 8(b) and 8(d)]. Another example of four line shapes for the interesting 1354.4-keV γ ray is shown in Figs. 9(a)–9(d). The line shape changes drastically as the bombardment energy is increased. In Figs. 8(a)–8(f) the solid lines are the calculated line shapes using the program SHAPES[15,16] assuming only one component since no other γ rays were observed to populate the levels deexcited by the γ rays in question. In all other cases the effect of population by known γ rays to the line shape was properly taken into account.[16] For each bombardment energy the feeding fractions and the corresponding effective lifetimes of the levels deexciting by the feeding transitions were used to obtain the theoretical line shape.

In Fig. 9 the solid lines show the calculated line shapes corrected for observed feeding with branchings and effective lifetimes τ_2 as shown. The τ_2 values were obtained from the smooth curves drawn through plots of the effective lifetime for each level which populates the level in question using the values summarized in Table IV as discussed below. The deduced effective lifetimes τ_1 shown in Fig. 9 for this level correspond to shapes that gave the minimum χ^2 values for the fit to the data.

The effective lifetimes of the levels analyzed after correction for the effect of observed γ feeding as a function of bombardment energy are plotted in Fig. 10. The effective lifetime becomes the level lifetime at the effective threshold. The effective lifetimes were extrapolated to the effective

thresholds shown by the vertical arrows in Fig. 10 by drawing smooth lines through the data.

Analyses of the observed line shapes by assuming that the levels are entirely populated via unobserved γ cascades do not improve the fits to the data of Fig. 9. The systematic observation of a valley between what appears to be the unshifted and the shifted components of the line shapes in Fig. 9 suggests the presence of considerable direct population by particle emission. In order to demonstrate the effect of such direct population we show in Fig. 11 the calculated line shapes for the 1355.4-keV γ ray for the two bombardment energies of 23.4 and 26.5 MeV using the partial decay schemes given in the inserts. The lifetime for the 3638-keV level was kept constant at 0.08 ps (Table IV), the effective lifetimes for the 4180-keV level at 23.4 and 26.5 MeV were kept constant at 0.63 and 0.68 ps, and the direct feedings were arbitrarily taken as 50 and 40%, respectively. The lifetime of the remaining unobserved cascade was varied to give the best fit to the data. It is quite clear from Fig. 11 that a remarkable improvement in the fits is obtained when sizable fractions of direct population are assumed. Of course, the statistical quality of the present data did not warrant a search for a meaningful best fit, by varying both the fraction and the unobserved cascade lifetime. Nonetheless, a significant fraction, perhaps in excess of 20%, appears to be present in this reaction for this 3638-keV 8_1^+ level.

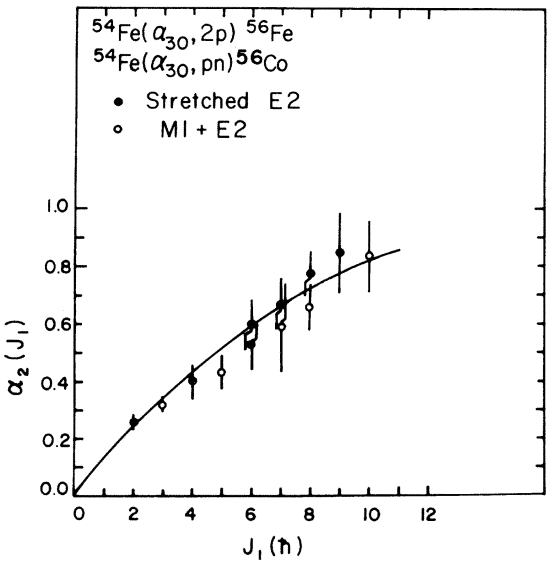

FIG. 6. Angular distribution attenuation coefficients for transitions in ^{56}Co and ^{56}Fe following α bombardment of ^{54}Fe at 29.5 MeV, plotted as a function of the level spin J_1. The closed circles are from stretched $E2$ transitions and the open circles from mixed $M1 + M2$ transitions.

The present results were also analyzed via the $F(\tau)$ or centroid shift method. Although the two methods should give the same result, small differences (<10%) are found due to the fact that in the line shape analysis the entire calculated distribution is fitted to the data, while in the centroid method only its first moment is compared with experiment. The present results are summarized in Table IV. The first two columns give the level and transition energy in keV, the third and fourth columns give the α-bombardment energy and the average initial velocity $\bar{\beta}(0)$ calculated from three body kinematics as described in Ref. 15, the fifth and sixth columns give $F(\tau)$ and effective lifetime τ in fs for the four bombardment energies employed, and the last column gives the proposed mean lifetime for each level. The effective lifetimes given in Table IV are weighted averages from the line shape and $F(\tau)$ analyses. The uncertainties given in the proposed level lifetimes include a substantial contribution for possible systematic error from the extrapolation. This significantly affects only the uncertainties for the 3638.0- and 5274.6-keV levels in ^{56}Co and the 3755.8-keV level in ^{56}Fe.

III. PROPOSED DECAY SCHEMES AND ASSIGNMENT OF J^π VALUES

From the evidence obtained in this work detailed schemes for the decay of many new yrast and some non-yrast levels in ^{56}Co and ^{56}Fe were constructed

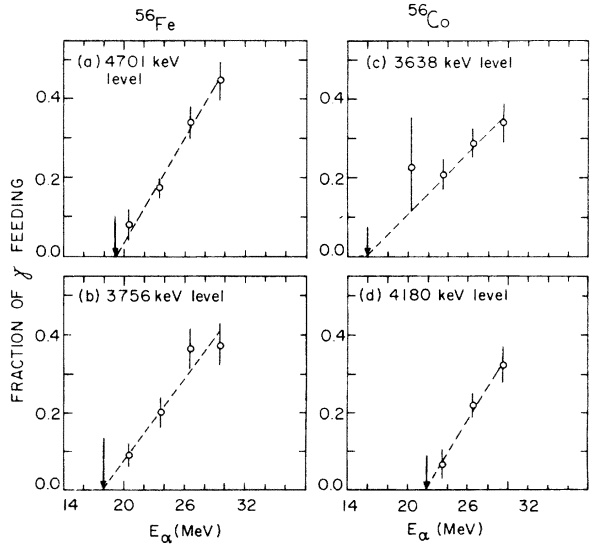

FIG. 7. Fraction of observed feeding to some levels in ^{56}Fe and ^{56}Co as a function of bombardment energy. The vertical arrows indicate the suggested effective threshold below which γ feeding from above is assumed to be insignificant.

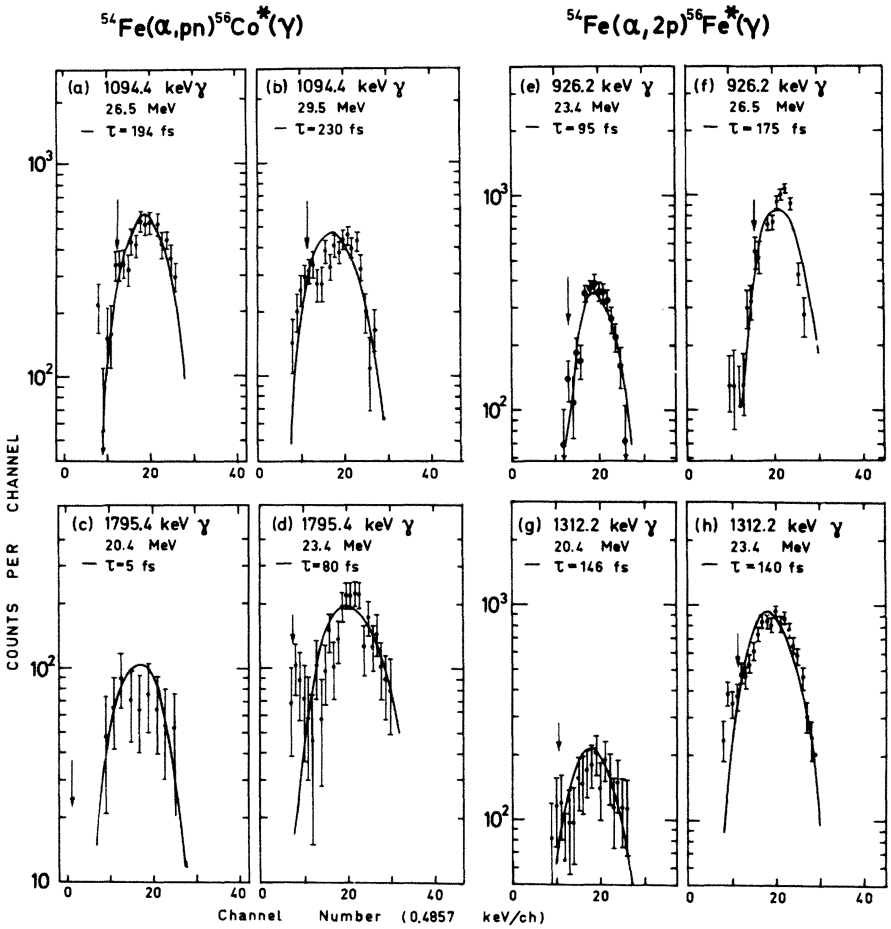

FIG. 8. Comparison of the calculated line shapes for the γ rays indicated with experimental data obtained in singles measurements at 55° to the beam. The effective lifetimes which gave the minimum χ^2 are shown in fs. The vertical arrows indicate the position of the unshifted line if emission were to occur at rest.

and are shown in Figs. 3 and 4. In what follows arguments for some of the new levels and J^π assignments will be given from evidence obtained in this work.

A. High-spin levels in ^{56}Co

The decay properties of the first five levels shown in Fig. 3 were well established in the work of Ref. 6.

The level at 2282.6 keV is definitely assigned as 7_1^+ on the basis of the angular distribution and excitation function for the 1706.0-keV γ ray [Figs. 5(d) and 2(a)]. The attenuation coefficient $\alpha_2(J_1)$ for this transition corroborates this assignment. This is also consistent with the $L=6$ assignment for the (d,α) work of Hjorth.[17] The lifetime for this level was found to be longer than 2 ps from lack of observable Doppler broadening.

A level at 2371.9 keV was observed to decay to the 576.47- and 1009.17-keV levels below. The angular distribution for the 1795.4-keV γ ray is consistent only with a dipole $6^+ \rightarrow 5^+$ transition. This level should be identified with the 2371-keV level assigned as $(6^+, 5^+, 7^+)$ by Schneider and Daehnick.[5] The lifetime for this level was found to be very short, namely, 0.06 ± 0.03 ps.

A new level at 3638.0 keV was found to deexcite only by the 1355.4-keV γ ray. The excitation function for this level is typical of a high-spin level, while the angular distribution for the 1355.4-keV γ ray is consistent with a dipole $8_1^+ \rightarrow 7_1^+$ transition with some $E2$ admixture [see Table III and Fig. 5(f)] and it is definitely not a stretched $9^+ \rightarrow 7^+$ transition. The very short lifetime of $0.08^{+0.04}_{-0.03}$ ps is consistent with the primarily dipole character for this transition.

A new level at 4180.2 keV was established to decay to the 2282.6- and 3638.0-keV levels below (Fig. 3). This level is definitely 9_1^+ as evidenced from the excitation function and angular distri-

bution for the 1898.0-keV γ ray [Figs. 2(a) and 5(g)].

Finally, a new level at 5274.6 keV is established in this work to decay only by the 1094.4-keV γ ray to the 9_1^+ level at 4180.2 keV. The excitation function [Figs. 2(a)] indicates a high-spin level, and the angular distribution of the 1094.4-keV γ ray indicates a dipole $10_1^+ \rightarrow 9_1^+$ rather than a stretched $E2$ transition [Fig. 5(i)]. The very short lifetime of $0.10^{+0.03}_{-0.02}$ ps is consistent with this assignment.

B. High-spin levels in ^{56}Fe

The decay properties of the first two levels shown in Fig. 4 are well established.[9]

A level at 3388.4 keV was confirmed in this work to deexcite primarily by a 1303.4-keV γ ray to the 4_1^+ level at 2085.08 keV, and by a weak 265.5-keV branch to the 4_2^+ level at 3122.9 keV.

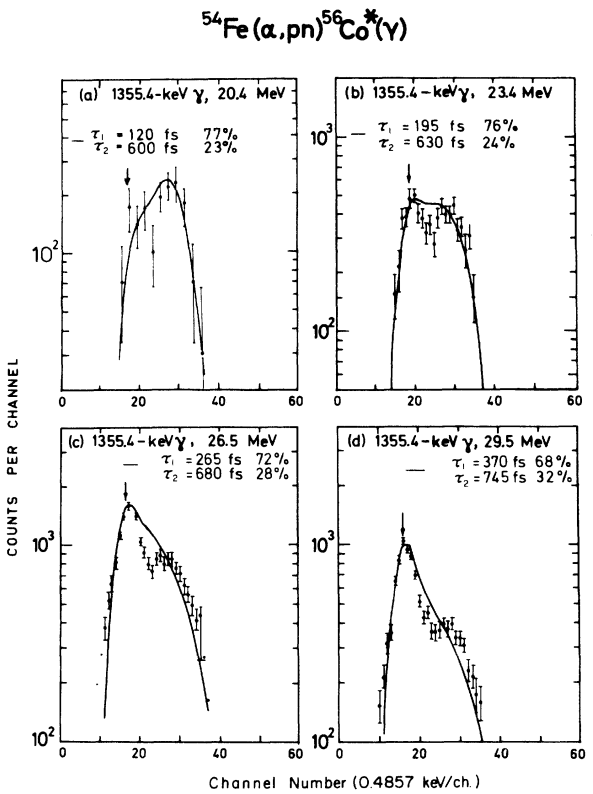

FIG. 9. Dependence on bombardment energy of the line shape of the 1355.4-keV γ ray in ^{56}Co observed in singles measurements at 55° to the beam direction. The effective lifetime τ_1 for the 3638-keV level deexciting by the 1355.4-keV γ ray was obtained for the calculated line shape shown and corresponds to a minimum χ^2 fit. The effective lifetime τ_2 of the 4180.2-keV level that decays to the 3638-keV level with the fraction indicated was kept constant at the value shown in the calculation of the line shape. A drastic change in shape is observed as the bombardment energy is increased.

The excitation function and angular distribution for the 1303.4-keV γ ray are consistent only with a stretched $E2$ transition assigned as $6_1^+ \rightarrow 4_1^+$. This is consistent with the assignment of Poletti *et al.*[2] as (6^+). A lower limit of 2 ps for the mean lifetime for this level can be placed for this lack of observable Doppler broadening in the thick target experiments.

A level at 3755.8 keV was confirmed here to decay to the 2085.08- and 3388.4-keV levels below. The angular distribution for the 1670.8-keV γ ray [Fig. 5(m)] is consistent only with a stretched $E2$ $6^+ \rightarrow 4^+$ transition and not with a $5^+ \rightarrow 4^+$ transition as assigned by Poletti *et al.*[2] The lifetime of $0.18^{+0.04}_{-0.03}$ ps measured in the present work is also in disagreement with the value of 3.4 ± 1.1 ps reported in Ref. 2.

A level at 4700.6 keV was confirmed to deexcite by two γ rays of 944.7 and 1312.2 keV. The excitation function for 1312.2-keV transition [Fig. 2(b)] is indicative of a high-spin state. The angular distribution [Fig. 5(n)] indicates a dipole transition (see Table V) and this limits the J^π assignment for this level to 7_1^+. A negative parity for this level would require a very fast $E1$ transition with a lifetime of $0.12^{+0.04}_{-0.02}$ ps and this is very unlikely.

A level at 5255.3 keV is found to decay by two γ rays of 1499.3 and 1867.1 keV. The excitation function for the 1867.1-keV γ ray [Fig. 2(b)] suggests a high J^π value and the angular distribution of the same γ ray [Fig. 5(o)] supports a stretched $E2$ transition. This limits the J^π value for this level to 8_1^+. A lifetime of 0.50 ± 0.05 ps was obtained for this level.

Finally the level at 5626.8 keV was confirmed to deexcite by the 926.2- and 2238-keV γ rays. The high J^π character of the excitation function [Fig. 2(b)] and the angular distribution [Fig. 5(p)] for the 926.2-keV γ rays limit this transition to $8_1^+ \rightarrow 7_1^+$. A J^π value of 8^- is excluded because of the rather large quadrupole admixture $\delta(E2/M1)$ of 0.25 ± 0.10 obtained for an $8 \rightarrow 7$ sequence and by the observed branch to the 6_1^+ level at 3388.4 keV. This level was found to have a lifetime of $0.10^{+0.03}_{-0.02}$ ps.

IV. REDUCED TRANSITION PROBABILITIES IN ^{56}Co AND ^{56}Fe

The measured branching ratios, multipole mixing ratios, and the level mean lifetimes presented in Tables I, III, and IV were used to obtain the reduced transition probabilities $B(E2)$ and $B(M1)$ for the electric quadrupole and magnetic dipole components for many of the transitions from high-spin states in ^{56}Co and ^{56}Fe. The results are summarized in Table V. The first two columns in Table V give the level energy in keV and the mean

TABLE IV. Summary of the deduced $F(\tau)$ values, effective lifetimes, and proposed lifetimes for levels in ^{56}Co and ^{56}Fe populated in the (α,pn) and $(\alpha,2p)$ reactions on ^{54}Fe for energies $E_\alpha = 20.4$–29.5 MeV obtained from singles experiments.

E_{level} (keV)	Transition (keV)	E_α (MeV)	$\bar{\beta}(0)$	$F(\tau)$	Effective τ (fs)	Proposed level τ (fs)
			^{56}Co			
2371.9	1795.4	20.4	0.007 406	0.97 ± 0.27	≤95	60 ± 30
		23.4	0.007 962	0.73 ± 0.04	80^{+16}_{-25}	
		26.5	0.008 493	0.55 ± 0.02	250 ± 35	
		29.5	0.008 979	0.548 ± 0.015	270 ± 21	
3638.0	1355.4	20.4	0.007 401	0.69 ± 0.21	120 ± 40	80^{+40}_{-30}
		23.4	0.007 951	0.47 ± 0.02	195 ± 30	
		26.5	0.008 473	0.43 ± 0.02	270 ± 30	
		29.5	0.008 962	0.33 ± 0.02	370 ± 70	
4180.2	542.0 and	20.4	0.007 401	0.258 ± 0.077	600 ± 100	590 ± 60
	1898.0	23.4	0.007 951	0.253 ± 0.017	621 ± 80	
		26.5	0.008 473	0.235 ± 0.018	694 ± 60	
		29.5	0.008 962	0.217 ± 0.015	746 ± 48	
5274.6	1094.4	23.4	0.007 940	0.85 ± 0.30	45^{+60}_{-45}	60^{+40}_{-20}
		26.5	0.008 449	0.52 ± 0.04	194 ± 30	
		29.5	0.008 939	0.56 ± 0.02	230 ± 30	
			^{56}Fe			
3755.8	1670.8	20.4	0.007 452	0.595 ± 0.019	250 ± 32	180^{+40}_{-30}
		23.4	0.008 010	0.398 ± 0.013	400 ± 47	
		26.5	0.008 534	0.306 ± 0.010	510 ± 55	
		29.5	0.009 015	0.262 ± 0.010	682 ± 39	
4700.6	1312.2	20.4	0.007 431	0.639 ± 0.032	146 ± 25	120^{+40}_{-20}
		23.4	0.008 004	0.601 ± 0.010	140 ± 18	
5255.3	1867.1	20.4	0.007 431	0.324 ± 0.089	500 ± 85	500 ± 50
		23.4	0.008 004	0.316 ± 0.017	570 ± 70	
		26.5	0.008 529	0.295 ± 0.022	610 ± 60	
		29.5	0.009 012	0.284 ± 0.009	700 ± 50	
5626.8	926.2	23.4	0.007 998	0.728 ± 0.045	95 ± 50	100^{+30}_{-20}
		26.5	0.008 523	0.499 ± 0.025	175 ± 30	

lifetimes in ps; the third and fourth columns give the transition energy in keV and the percent branching; the fifth column gives the proposed spin sequence; the sixth column gives the experimental $\delta(E2/M1)$ values employed; and the eighth and tenth columns give the $B(E2)$ and $B(M1)$ values in Weisskopf units (W.u.). The $B(\Lambda)$ values were calculated as described in the Appendix of Ref. 18. For a more meaningful comparison with theory, measured $B(\Lambda)$ values for transitions from the lower-spin states have been included in Table V and these are footnoted accordingly.

The $B(\Lambda)$ values determined for the high-spin states in ^{56}Co and ^{56}Fe depend in some cases on the $\delta(E2/M1)$ values used. The latter in turn depend on the attenuation factor $\alpha_2(J_1)$ used (see Table III) in the analysis of the measured angular distributions in order to extract the $\delta(E2/M1)$ value. In these cases the $\alpha_2(J_1)$ values deduced in a minimum χ^2 search as a function of δ and σ were found within experimental error near the empirical curve of Fig. 6 which is based on the $\alpha_2(J_1)$ values from known and assigned stretched $E2$ transitions (see Table III).

V. COMPARISON WITH THEORY AND DISCUSSION

A. $^{56}_{26}Fe_{30}$ nucleus

The structure of the low-lying levels in the ^{56}Fe nucleus have been interpreted by Horie and Ogawa[1] in terms of the $(\pi 1f_{7/2})^6(\nu 2p_{3/2}, \nu 2p_{1/2}, \nu 1f_{5/2})^2$ configuration. By using proton-neutron effective interaction matrix elements derived from $N=29$ nuclei outside a ^{48}Ca inert core, these authors[1] calculated the level spectra of a number of nuclei including ^{52}Ti, ^{54}Cr, and ^{56}Fe. In Fig. 11 these predictions are compared with the results from this experiment. It is interesting to note that the

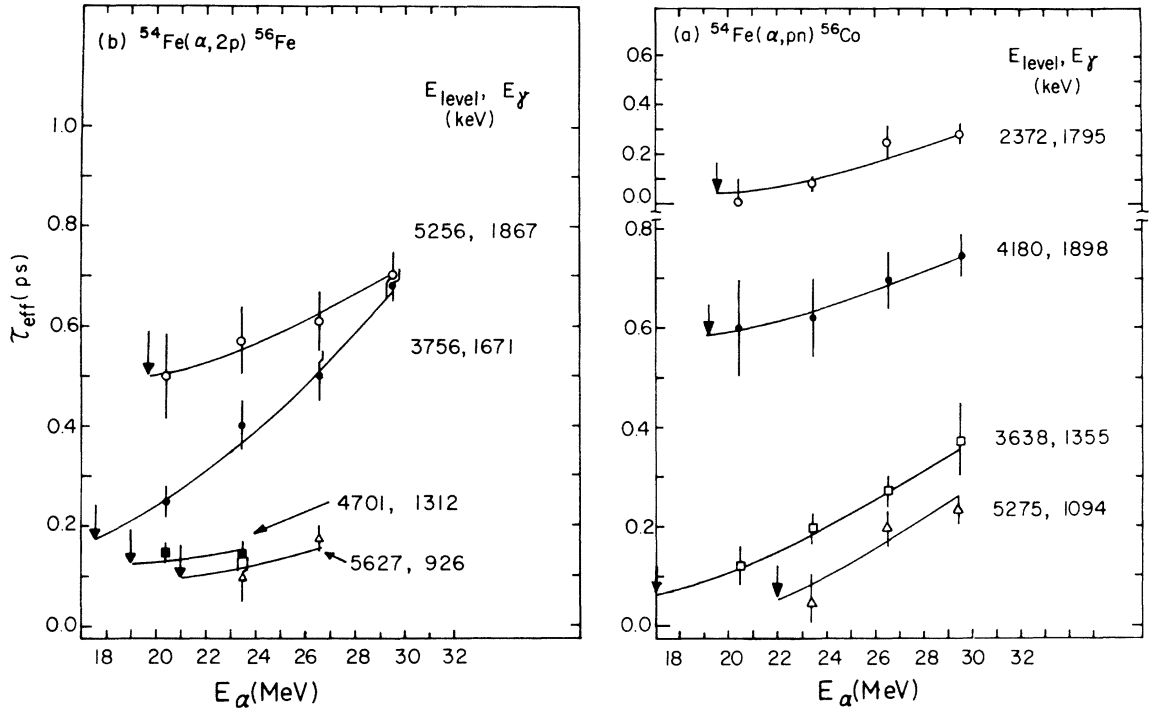

FIG. 10. Plots of the extracted effective mean lifetimes vs α-bombardment energy for the transitions in ^{56}Fe and ^{56}Co indicated. The vertical arrows show the projectile energies below which γ rays feeding the levels in question could not be observed. The proposed mean lifetimes for the levels analyzed were obtained by extrapolation to these bombardment energies with smooth lines through the data.

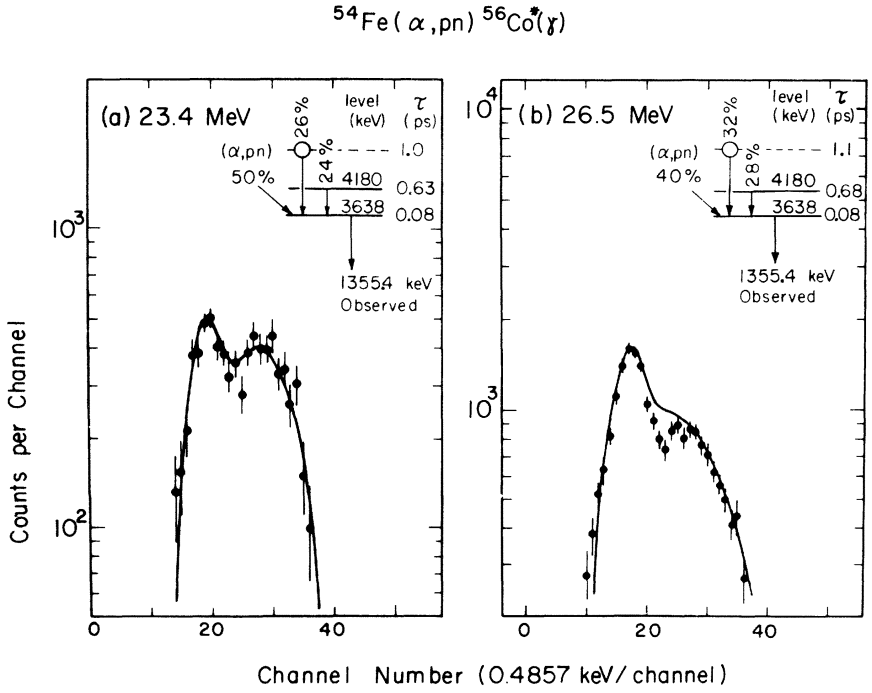

FIG. 11. Comparison with experiment of the calculated line shapes for the 1355.4-keV γ ray at the bombardment energies given by employing the partial decay schemes shown as inserts. It is seen that the improvement in the fits compared with Figs. 8(b) and 8(c) is due to the inclusion of a direct population component.

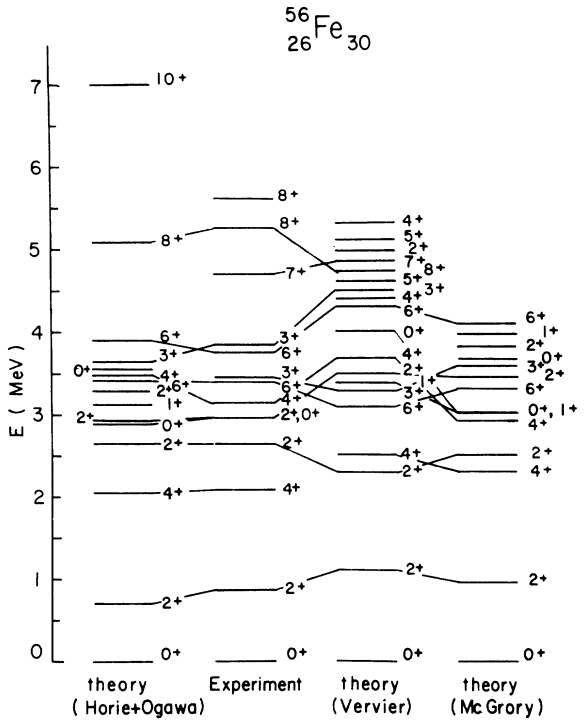

FIG. 12. Comparison of the experimental level spectrum of ^{56}Fe with the results of various shell model calculations for this nucleus.

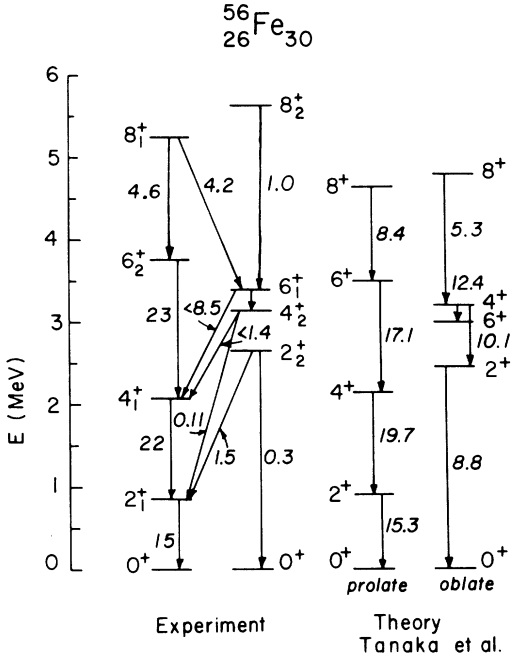

FIG. 13. Comparison of the experimental level structure and transition rates for ^{56}Fe with the calculations of Tanaka and Sheline. The transition rates are given in W.u. next to the transition arrows. Coexistence of configurations with prolate- and oblate-like quasiband structure is suggested from this comparison.

agreement is quite good if one considered the 6_1^+, 6_2^+, and 8_1^+ states in particular. It should be noted here that the position of the higher-spin states other than the 8_1^+ and 10_1^+ was not reported by Horie and Ogawa.[1] Transition probabilities from these calculations[1] for the first two excited states have been quoted by Poletti *et al.*[2] and reproduce well the experimental values.[2] In Fig. 12 is also shown a comparison of the level sequence in ^{56}Fe with the results of an earlier calculation by Vervier[19] based on a δ-function radial dependence of the effective nucleon-nucleon interaction. The results of a more extensive shell-model calculation by McGrory[20] are also shown in Fig. 12. Qualitative agreement with experiment is observed from the comparisons shown in Fig. 12.

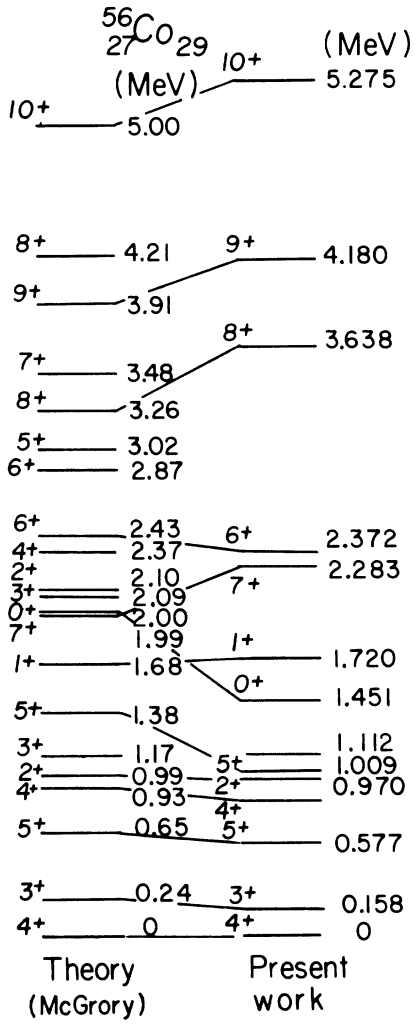

FIG. 14. Comparison of the level structure with the result of the shell-model calculation by McGrory. The order of the high-spin states is correctly predicted.

TABLE V. Summary of the electromagnetic properties of transitions observed in ^{56}Co and ^{56}Fe and comparison with theory.

E_{level} (keV)	τ_{level} (ps)	Transition (keV)	Branching (%)	$J_i^\pi \rightarrow J_f^\pi$	Multipole mixing ratio $\delta(E2/M1)$	Reduced transition probabilities $B(E2)$ in W.u. Exp.	$B(E2)$ Theory[a]	$B(M1)$ in W.u. Exp.	$B(M1)$ Theory[a]
				^{56}Co					
158.38 10[b]	≤144[c]	158.38 10	100	$3_1^+ \rightarrow 4_1^+$	−0.07 6[d]		3.1		0.73
576.50 7[b]	0.48^{+22}_{-11}[e]	576.64 19	100	$5_1^+ \rightarrow 4_1^+$	0.061 16[d]	7.8^{+52}_{-43}	3.2	0.34^{+10}_{-11}	0.25
829.58 6[b]	>2.4[f]	252.9 2	1.5 2[g]	$4_2^+ \rightarrow 5_1^+$	$(M1)$[h]		3.2	(≤0.012)	0.027
		671.4 4	74.5 12[g]	$4_2^+ \rightarrow 3_1^+$	0.24 3[d]	≤4.5	2.0	≤0.031	0.0071
		830.1 2	24.0 9[g]	$4_2^+ \rightarrow 4_1^+$	$(M1)$[h]		1.3	(≤0.0055)	0.0011
970.25 11[i]	0.11^{+3}_{-2}[e]	811.8 1	99.7 56[i]	$2_1^+ \rightarrow 3_1^+$	0.025 15[j]	1.0^{+16}_{-9}	0.21	0.54 12	0.29
		970.4 2	0.30 5[i]	$2_1^+ \rightarrow 4_1^+$	$E2$	2.0^{+5}_{-7}	0.18		
1009.17 6[b]	0.47^{+21}_{-11}[e]	179.5 2	3.7 4[g]	$5_2^+ \rightarrow 4_2^+$	$(M1)$[h]		4.5	(0.43 13)	0.29
		432.7 2	6.6 4[g]	$5_2^+ \rightarrow 5_1^+$	$(M1)$[h]		0.010	(0.055 17)	0.031
		1009.3 2	89.7 12[g]	$5_2^+ \rightarrow 4_1^+$	0.11 5[j]	1.4^{+16}_{-10}	1.6	0.058 18	0.16
1114.48 6[i]	0.34^{+5}_{-3}[e]	284.86 10[i]	11.4 10[k]	$3_2^+ \rightarrow 4_2^+$	0.03 5[j]	7^{+70}_{-7}	3.4	0.46^{+5}_{-7}	0.36
		956.14 8[i]	4.8 3[k]	$3_2^+ \rightarrow 3_1^+$	$(M1)$[h]		0.26	(0.0051 6)	0.011
		1114.47 8[i]	84.8 17[k]	$3_2^+ \rightarrow 4_1^+$	−0.085 25[j]	8.5^{+57}_{-44}	0.38	0.057^{+7}_{-8}	0.013
1450.62 14[i]	2300 140[c]	480.37 8[i]	100	$0_1^+ \rightarrow 2_1^+$	$E2$	1.08 7	0.20		
1720.12 9[e]	0.57^{+38}_{-14}[e]	269.44 10[i]	36.6 23[k]	$1_1^+ \rightarrow 0_1^+$	$M1$			1.0^{+4}_{-5}	1.46
		749.89 8[i]	50.7 26[k]	$1_1^+ \rightarrow 2_1^+$	0.10 15[j]	≤19	0.17	0.066^{+22}_{-27}	0.0024
		1561.8 2[i]	12.7 8[k]	$1_1^+ \rightarrow 3_1^+$	$E2$	1.5^{+5}_{-6}	0.033		
2282.6 2	>2.0	1706.1 1	100	$7_1^+ \rightarrow 5_1^+$	$E2$	<2.2	0.019		
2371.9 2	0.06 ± 0.03	1362.0 5	28 3	$6_1^+ \rightarrow 5_2^+$	$(M1)$[h]		1.5	(0.059^{+59}_{-30})	0.055
		1795.4 2	72 6	$6_1^+ \rightarrow 5_1^+$	−0.03 5	≤0.5	4.1	0.066^{+66}_{-33}	0.12
3638.0 2	0.08^{+4}_{-3}	1355.4 1	100	$8_1^+ \rightarrow 7_1^+$	−0.15 4	3.9^{+33}_{-22}		0.16^{+9}_{-5}	
4180.2 2	0.59 6	542.0 1	27 1	$9_1^+ \rightarrow 8_1^+$	−0.05 9	<12		0.091^{+10}_{-8}	
		1898.0 3	73 3	$9_1^+ \rightarrow 7_1^+$	$E2$	3.2^{+4}_{-3}			
5274.6 3	0.06^{+4}_{-2}	1094.4 1	100	$10_1^+ \rightarrow 9_1^+$	−0.13 5	11^{+23}_{-3}		0.40^{+40}_{-13}	
				^{56}Fe					
846.75 4	9.7 3[l]	846.75 4	100	$2_1^+ \rightarrow 0_1^+$	$E2$	15.2 5	15.3		
2085.05 6	$1.0^{+0.6}_{-0.3}$[l]	1238.30 4	100	$4_1^+ \rightarrow 2_1^+$	$E2$	22^{+9}_{-8}	19.7		
2657.8 2	0.040 10[l]	1810.8 2	97.8[l]	$2_2^+ \rightarrow 2_1^+$	0.14 3	1.5^{+5}_{-8}		0.14^{+4}_{-3}	
		2657.8 2	2.2[l]	$2_2^+ \rightarrow 0_1^+$	$E2$	0.26^{+9}_{-5}	8.8		
3122.9 1		1037.8 1	99.1[l] 7[l]	$4_2^+ \rightarrow 4_1^+$	0.01 4	≤1.4[l]		0.43^{+71}_{-22}[l]	
		2276.3 2	0.93 8[l]	$4_2^+ \rightarrow 2_1^+$	$E2$	0.11			

TABLE V. (*Continued*)

E_{level} (keV)	τ_{level} (ps)	Transition (keV)	Branching (%)	$J_i^\pi \rightarrow J_f^\pi$	Multipole mixing ratio $\delta(E2/M1)$	Reduced transition probabilities $B(E2)$ in W.u. Exp.	$B(E2)$ Theory[a]	$B(M1)$ in W.u. Exp.	$B(M1)$ Theory[a]
				^{56}Fe					
3388.4 1	>2.0	265.5 2	1.3 3	$6_1^+ \rightarrow 4_2^+$	$E2$	≤ 320	8.6		
		1303.4 1	98.7 40	$6_1^+ \rightarrow 4_1^+$	$E2$	≤ 8.5			
3755.5 2	0.18^{+4}_{-2}	367.0 2	18 1	$6_2^+ \rightarrow 6_1^+$	+0.07 12	≤ 300		0.62^{+8}_{-12}	
		632.6	<1.3	$6_2^+ \rightarrow 4_2^+$	$E2$	≤ 47			
		1670.8 4	82 3	$6_2^+ \rightarrow 4_1^+$	$E2$	23^{+3}_{-4}	17.1		
4700.6 2	0.12^{+4}_{-2}	944.7 2	16 2	$7_1^+ \rightarrow 6_2^+$	$(M1)$[h]			(0.050^{+10}_{-13})	
		1312.2 1	84 4	$7_1^+ \rightarrow 6_1^+$	−0.08 8	≤ 3.4		0.10^{+2}_{-3}	
5255.3 3	0.50 5	1499.3 3	27 3	$8_1^+ \rightarrow 6_2^+$	$E2$	4.6^{+6}_{-5}	8.4		
		1867.1 2	73 4	$8_1^+ \rightarrow 6_1^+$	$E2$	4.2^{+5}_{-4}			
5626.8 3	0.10^{+3}_{-2}	926.2 1	91.7 14	$8_2^+ \rightarrow 7_1^+$	0.25 10	50^{+44}_{-34}		0.35 8	
		1871.3	<10	$8_2^+ \rightarrow 6_2^+$	$E2$	<35			
		2238 2	8.3 20	$8_2^+ \rightarrow 6_1^+$	$E2$	1.0 ± 5	5.3		

[a] Theoretical values for ^{56}Co are from Ref. 3 and for ^{56}Fe from Ref. 8.
[b] Weighted average from this work and Ref. 6.
[c] D. O. Wells, S. L. Blatt, and W. E. Meyerhof, Phys. Rev. 130, 1961 (1963).
[d] Weighted average from this work (Table III) and Ref. 4.
[e] Weighted average from Refs. 6 and 7.
[f] From Ref. 7.
[g] Weighted average from this work and Refs. 6 and 7.
[h] Assumed pure $M1$.
[i] From Ref. 6.
[j] From Ref. 4 taken at the midpoint of the range given with equal upper and lower uncertainties.
[k] Weighted average from Refs. 4 and 6.
[l] From Ref. 9.

In a recent paper Tanaka and Sheline[8] reported calculations for ^{56}Fe based on the aligned coupling scheme used to construct wave functions from spherical bases in order to explain possible quasiband structures. From these calculations configurations arise which exhibit prolate- or oblate-like structures.[8] In Fig. 13 we show a comparison of the level sequence and electromagnetic decay properties of the high-spin states in ^{56}Fe as determined in this work with the results of Tanaka and Sheline.[8] The similarity in the level structures labeled[8] as prolate and oblate (Fig. 13) with the experimental ones is a striking one and may suggest a coexistence of configurations with such shapes. This suggestion is considerably strengthened by a close comparison of experimental and theoretical $B(E2)$ values which are given in W.u. near the appropriate arrows characterizing each transition. First, we point out the striking agreement of the measured and calculated $B(E2)$ values for the so-called prolate-like quasiband structure. The measured quadrupole moment[21] for the 2_1^+ state in ^{56}Fe further substantiates a "stiff prolate rotor" for ^{56}Fe in this state. The interpretation of the $2_2^+, 4_2^+, 6_1^+, 8_2^+$ sequence in ^{56}Fe (see Fig. 13) as a possible oblate-like structure may be based (a) on the level sequence and (b) on the following transition rate information. The 6_1^+ state at 3388.4 keV was found to be long-lived ($\tau \geq 2.0$ ps). The ratio $B(E2; 6_1^+ \rightarrow 4_1^+)/B(E2; 6_1^+ \rightarrow 4_2^+)$ was found from the relative intensities for these transitions to be 0.027 ± 0.006 indicating a significant retardation for the decay from the oblate- to the prolate-like shape. Such a behavior supports the interpretation of this 6_1^+ state as a shape isomer. Although the $4_2^+ \rightarrow 4_1^+$ and $2_2^+ \rightarrow 2_1^+$ transitions (Fig. 12) are slow[22] and further support the coexistence of the shape isomeric structures, one may well expect

considerable interaction between the two shapes, thus resulting in mixing of the respective wave functions. Consequently, transitions such as the $8_1^+ \rightarrow 6_1^+$ with $B(E2) = 4.2$ W.u. are not surprising. The slow $B(E2;\ 2_2^+ \rightarrow 0^+) = 0.3$-W.u. transition may also be explained by raising the question of the nature of the 0^+ ground state and by the possibility of considerable two-phonon character in the 2_2^+ state which will retard the transition to ground.

B. $^{56}_{27}Co_{29}$ nucleus

In the interpretation of the structure of this nucleus it has been shown by Schneider and Daehnick[5] that one-particle–one-hole description is not sufficient to explain the (d, α) and $(^3He, p)$ results, but that admixtures of two-particle–two-hole configurations to most of the ^{56}Co states is important. Recently, results of calculations by McGrory as quoted in Ref. 4 were compared with experiment by Barker and Sarantites[6] and by Moazed *et al.*[7] In these calculations[3] ^{56}Co is described by a ^{40}Ca core with 14 or 15 nucleons in the $f_{7/2}$ orbit with the remaining in the $p_{3/2}$, $f_{5/2}$, or $p_{1/2}$ orbits. Single-particle energies which reproduce best the ^{57}Ni spectrum and Kuo-Brown matrix elements for the effective two-body interaction were used and the calculations were extended[3] to the high-spin states up to J^π of 10^+. The results are compared with the experimental level spectrum in Fig. 14 where only the first levels calculated for each J^π value are shown. It is interesting to note that the observed sequence for the high-spin states is predicted by the calculations.[3] With the wave functions that give the results shown in Fig. 14 the $B(M1)$ values were calculated using the bare proton value for the $M1$ operator. The calculated $B(M1)$ values were found to overestimate the observed transition rates by a factor of about 3–4. The calculated $B(M1)$ values for transitions in ^{56}Co shown in the last column of Table V refer to an effective charge of 0.5. The comparison of Table V indicates that an effective charge of 0.5–0.6 reproduces the observed transition rates best. The $B(E2)$ values were also calculated with an effective charge of 0.5 and this gives a reasonable agreement with experiment.

Note added: After this article was submitted for publication, Bendjaballah *et al.*[23] published results of a similar investigation. Excellent agreement with the present results for ^{56}Fe is observed.

ACKNOWLEDGMENTS

The excellent cooperation of the staff of the Washington University cyclotron is appreciated. One of the authors (DGS) expresses his thanks for the warm hospitality of all the members of the Research Institute for Physics in Stockholm where the last stages of this work were carried out. The authors also express their thanks to Professor E. S. Macias for this interest in this work and for stimulating discussions. We also thank Dr. J. B. McGrory for communicating the calculations for ^{56}Co.

---

*Work supported in part by the U. S. Atomic Energy Commission under Contract No. AT(11-1)-1530 and the Energy Research and Development Administration Contract No. E(11-1)-1760.

[1]H. Horie and K. Ogawa, Progr. Theor. Phys. 46, 439 (1971); Nucl. Phys. A216, 407 (1973).
[2]A. R. Poletti, B. A. Brown, D. B. Fossan, and E. K. Warburton, Phys. Rev. C 10, 2329 (1974).
[3]J. B. McGrory (private communication).
[4]L. E. Samuelson, W. H. Kelly, R. R. Todd, R. A. Warner, W. C. McHarris, F. M. Bernthal, E. M. Bernstein, and R. Shaum, Phys. Rev. C 7, 2379 (1973).
[5]M. J. Schneider and W. W. Daehnick, Phys. Rev. C 4, 1649 (1971).
[6]J. H. Barker and D. G. Sarantites, Phys. Rev. C 10, 1407 (1974).
[7]C. Moazed, J. C. Lawson, W. E. Dorenbusch, N. Schneiders, L. Weisman, and D. Voges, Nucl. Phys. A239, 242 (1975).
[8]Y. Tanaka and R. K. Sheline, Phys. Lett. 56B, 309 (1975).
[9]M. N. Rao, Nucl. Data B3, 4 (1970).
[10]D. G. Sarantites and W. G. Winn, Nucl. Phys. A172, 395 (1971).
[11]M. E. Phelps, D. G. Sarantites, and W. G. Winn, Nucl. Phys. A149, 647 (1970).
[12]D. G. Sarantites and E. J. Hoffman, Nucl. Phys. A180, 177 (1972); N.-H. Lu, Ph.D. thesis, Washington University, 1974 (unpublished).
[13]D. G. Sarantites, Phys. Rev. C 12, 1176 (1975).
[14]Z. Sawa and M. Anderson, as modified by D. G. Sarantites and M. Anderson (unpublished).
[15]J. Urbon, D. G. Sarantites, and L. L. Rutledge, Jr., Nucl. Instrum. Methods 126, 49 (1975).
[16]E. J. Hoffman, D. M. Van Petter, D. G. Sarantites, and J. H. Barker, Nucl. Instrum. Methods 109, 3 (1973).
[17]S. A. Hjorth, Ark. Fys. 33, 147 (1967).
[18]D. G. Sarantites, J. H. Barker, N.-H. Lu, E. J. Hoffman, and D. M. Van Patter, Phys. Rev. C 8, 629 (1973).
[19]J. Vervier, Nucl. Phys. 78, 497 (1966).
[20]J. B. McGrory, Phys. Rev. 160, 915 (1967).
[21]P. M. S. Lesser, D. Cline, P. Goode, and R. N. Horoshko, Nucl. Phys. A190, 597 (1972).
[22]Y. K. Agarwal, S. Hoffmann, and K. Wien, Nucl. Phys. A176, 142 (1971).
[23]N. Bendjaballah, J. Delaunay, T. Nomura, and H. J. Kim, Phys. Rev. Lett. 36, 1536 (1976).